Research Article Vol. 1, No. 8 / 15 Aug 2022 / Optics Continuum 1730
OPTICS CONTINUUM

Spatial mapping of bleaching in a metal-organic plasmon converter

MARTIN ROTHE,[1,*] YUHANG ZHAO,[2] HENRY HALIM,[2] YAN LU,[2,3] AND OLIVER BENSON[1]

[1]Humboldt-Universität zu Berlin, Institut für Physik & IRIS Adlershof, Newtonstraße 15, 12489, Berlin, Germany
[2]Helmholtz Zentrum Berlin für Materialien und Energie, Institute of Soft Matter and Functional Materials, Hahn-Meitner-Platz 1, 14109, Berlin, Germany
[3]Institute of Chemistry, University of Potsdam, 14476, Potsdam, Germany
[*]rothe@physik.hu-berlin.de

Abstract: Hybrid nanophotonic elements, fabricated by organic and inorganic materials, are going to be key components of modern devices. Coupled systems of photoemitters with a plasmonic waveguide serve the demand for nanoscopic frequency converters. However, processes like the degradation of the photoemitters via photobleaching occur and need to be monitored and controlled, to realize future successful devices. We introduce a hybrid perylene-diimide / silver nanowire as plasmon frequency converter. A versatile method is presented to monitor and analyze the bleaching process. It is based on a time series of photoluminescence images, during the operation of a single converter. An analytical model is applied on the data and unveils that the photobleaching rate is constant and independent of the operation of the plasmon converter.

1. Introduction

Integrated optical circuits on the micro- and nanometer length scale involving different material platforms are currently on the way from lab demonstrations to real devices. An active research direction is to exploit quantum effects to achieve improved sensitivity, security or computational power [1]. For these applications, generation, routing, interaction, and detection of elementary electromagnetic excitations in integrated circuits is required. In addition, non-linear interaction must be implemented. In order to achieve these functionalities the electromagnetic fields must be well designed and confined to achieve a good operation efficiency. Complementary approaches utilize either dielectric [2–4] or metallic nanostructures [5–8]. The latter support collective excitations of charge density oscillations and propagating electromagnetic waves, i.e., surface plasmon polaritons [9]. Various elements, such as sub-diffractive waveguides [10,11], resonators [12,13], and antennas [14] have been realized. More complex potential building blocks are, e.g., plasmon junctions [15], mode analysers [16], and chiral routers [17]. Individual plasmonic excitations and eventually their interaction can be achieved or mediated by coupling optically active organic molecules to a passive plasmonic circuit structure [15,18]. Compared to other emitters in the condensed phase, such as defect centers in diamond [19], molecules can be brought very close to surfaces leading to a large interaction with evanescent fields [20]. However, organic molecules typically show a limited amount of photoluminescence (PL) cycles until they degrade and bleach [21–25]. This is not only a property of the molecules themselves, but depends also strongly on the environment. For example, solvent dependent photo-oxidization of dissolved perylene-diimide derivatives (PDI) have been reported [26,27], as well as a correlation between the photostability and the used solvents during the fabrication of solid-state PDI films [28]. Furthermore, the bleaching rate of polymer-embedded terylene-diimide correlates with the oxygen permability of the surrounding matrix [29].

#454911 https://doi.org/10.1364/OPTCON.454911
Journal © 2022 Received 27 Jan 2022; accepted 17 May 2022; published 1 Aug 2022

OPTICS CONTINUUM

The PL of such a rylene dye in a hybrid environment, can be described by a Jablonski diagram [21,22], as shown in Fig. 1(a). After excitation of the system to an excited state (green arrow), Stokes-shifted radiative decay back into the ground state may occur (red arrow). An emitter is efficient, when the radiative decay is much more likely than a competing non-radiative decay (black arrow). In addition, an intersystem crossing (ISC) can occur, which changes the electronic system, e.g., from a singlet state (S) to a triplet state (T). In order to include degradation or bleaching, a final photo-product state (PP) is introduced in the model in Fig. 1(a) as well. The exact pathway to the PP state can include transitions through other intermediate dark states, can be triggered by additional photon absorption, may be excitation wavelength dependent and depends on the environment [22]. In the close vicinity of a plasmonic nanowire (NW, Fig. 1(a)), the absorption and emission of propagating plasmons provides an additional decay channel [23]. Due to a strongly enhanced density of states near the tightly confined electromagnetic field near the wire, i.e., the Purcell effect [30], the radiative decay rate to generate a photon or a propagating plasmon is increased with respect to the non-radiative transitions. Due to spin-orbit coupling in the plasmonic near-field, even the spin-forbidden transitions are influenced [31]. Concerning this complexity, the common assumption that the bleaching of emitters in hybrid systems follow a linear dependence with the excitation power [24,25], requires a review.

In this paper, we analyze photobleaching in a prototypical nanophotonic element, a plasmonic frequency converter. Conversion is an important functionality in order to match the frequency of a propagating plasmon to another functional element or to facilitate optical detection of plasmons in the far-field [17]. Figure 1(b) shows a schematic of the converter. It relies on incoherent frequency conversion [32]. A focused laser excites propagating plasmons on one end of a hybrid modified-perylene-diimide (MPDI) / silver nanowire (NW). The synthesis, the precise morphology, and the plasmon routing capabilities of these NWs are described elsewhere [17]. Plasmons are absorbed by MPDI molecules in a silica shell around the NW followed by a Stokes-shifted reemission. Finally, plasmons are scattered into photons at the end of the NW and can be detected in the far-field (see Supplement 1 for absorption data and the microscopy setup scheme). Besides plasmon frequency-conversion, the MPDI molecules may also directly emit photons, which allows to track the plasmon intensity along the nanowire (Fig. 1(c)). Figure 1(d) shows a typical transmission electron microscopy (TEM) image of one end of a hybrid NW. Single NWs, localized by dark-field imaging (DF, Fig. 1(e)) in our optical setup, show the typical spectral PL characteristics [17], when excited by a focused laser at 532 nm on one end of the NW (Fig. 1(f)). The spectrum appears homogeneous over the whole length with pronounced coupling spots for the frequency-converted plasmons at the ends.

The practical limitations of such a hybrid plasmon converter may be caused by plasmon damping in the silver wire, imperfections of design (e.g., thickness and uniformity of silica shell), quenching of the molecules due to agglomeration, and finally bleaching of the molecules. Here, we are particularly interested in bleaching, which can be quantified by the photobleaching rate. It determines the total number of photons (or plasmons) that a molecule has emitted before it irreversibly degrades [23]. The photobleaching rate is independent of the excitation power, if the bleaching cascade is triggered only by a single-photon absorption. In case of non-linear absorption, e.g., an instantaneous or consecutive two-photon (or two-plasmon) absorption, then the power law of the bleaching process differs from the linear PL power law. In consequence, the photobleaching rate becomes excitation power dependent. Therefore, observation of the photobleaching rate shines light on the degradation cascade. The excitation probability of the MPDI by plasmon absorption decays nearly exponentially along the NW and follows any additional modification of the plasmon density. For this reason, it is crucial to map the bleaching process along the NW. We perform this mapping by detecting the fluorescence of the MPDI in the silica shell surrounding the plasmonic NW. We investigate bleaching in the plasmon converter in both a dry nitrogen atmosphere as well as ambient environmental conditions. The experimental

OPTICS CONTINUUM

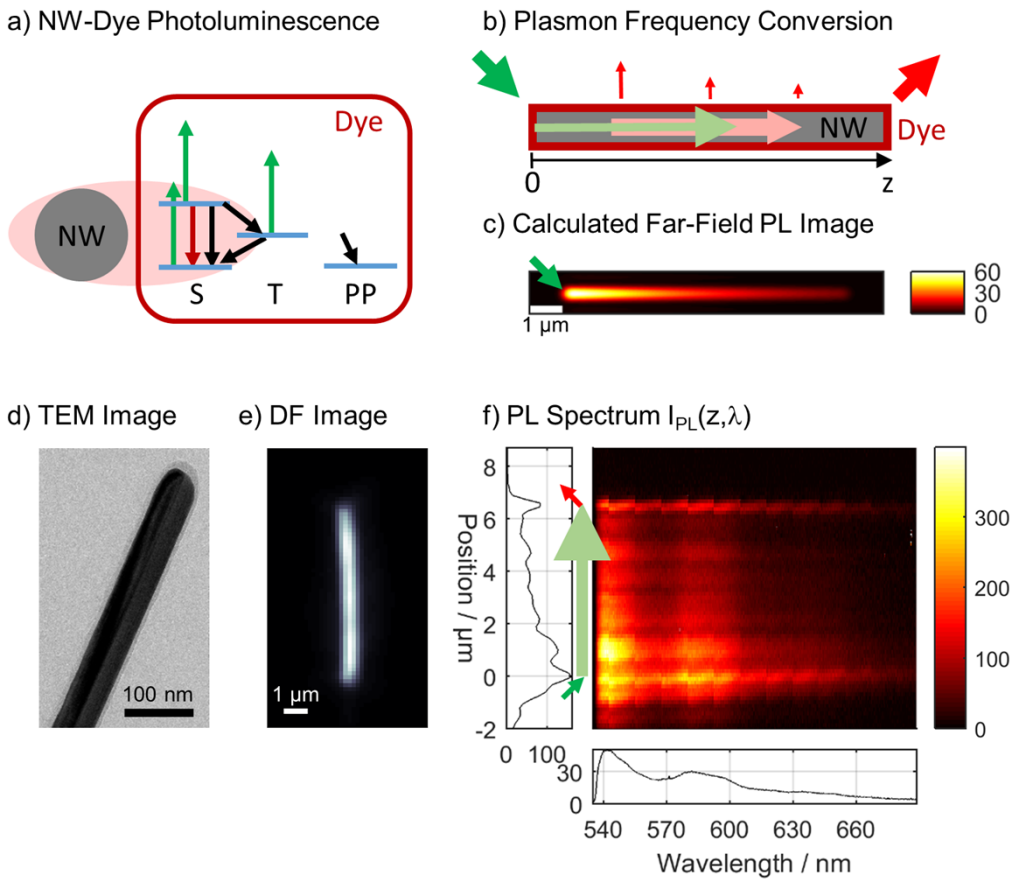

Fig. 1. Operating principle and characterization of the plasmon frequency converter. (a) A Jablonski diagram, depicting single or multiple excitation of a dye molecule (green arrows), and subsequent radiative (red) and non-radiative (black) decay channels. ISC may convert the electronic singlet (S) into a triplet system (T). A transition into the photo-product state (PP) represents irreversible bleaching. In the near-field of a plasmonic nanowire (NW) competing radiative and non-radiative transition probabilities change strongly. (b) Focused illumination on the left end of the NW (green arrow) excites the propagating plasmon (light-green arrow), which is then frequency-converted (light-red arrow), and scatters into photons on the right end (red arrow). Besides this, also direct photon emission (small red arrow) occurs. (c) According to the exponential damping of the propagating plasmons, the directly emitted photons form an image in the optical system. (d) The TEM image shows the precise morphology of a hybrid core-shell NW. (e) Dark-field imaging allows the localization of a single NW in the optical setup. (f) The same NW under focused laser illumination on the lower end shows the typical spectral characteristics of the MPDI as well as the spatial plasmon damping and the out-coupling of the frequency-converted plasmons.

OPTICS CONTINUUM

studies are accompanied by presenting a universal analytical model that allows to discriminate between linear and non-linear bleaching processes.

2. Experimental results

Hybrid silver nanowires of approximately 7 µm length and 70 nm width, with an 8 nm thick silica shell, and covalently bound MPDI molecules were chemically synthesized as described elsewhere [17]. The nanowires were spin-coated on a clean cover-glass, were located by dark-field imaging, and investigated by wide-field PL imaging in our home-built optical setup (see Supplement 1).

A cw-laser operating at 532 nm wavelength was focused on one end in order to excite plasmons propagating along the nanowire. The emission from the dye molecules in the shell surrounding the NW was recorded after suppressing the excitation light by approximately 10 orders of magnitude using two "Omega 538ALP" long-pass filters. Each consecutive series consist of 80 PL images with an acquisition time of 30s, respectively.

In order to limit ambient effects, a first series of PL images was recorded under dry nitrogen gas atmosphere. Figure 2(a) gives the first image of the consecutive series. A very bright spot appears in the upper left corner, where the focused laser is pointed at. Another bright spot appears in the lower right corner due to the frequency-converted plasmons, which scatter out at the NW ends. In between, the image shows directly emitted photons from the PL process, which are only partly overshown by the bright spots. Figure 2(b) gives the last image of the series. The full series can be found in the Supplement 1. In the last image, the lower right spot is darker by more than one order of magnitude compared to the spot in the first image. Although conversion is still going on, this reduction marks the slow approach towards the end of the lifetime of the building block.

We move on to the analysis of the bleaching process. The drop of PL intensity also appears along the full length of the nanowire. An exponential function describes the temporal evolution of each pixel (see section 3, analytical model)

$$I(x, y, t) = A \exp(-Bt) + C \tag{1}$$

Every pixel located at (x,y), which contributes substantial intensity, is fitted accordingly. The parameter C corrects for additional background, e.g., by overshining of the excitation light. It is a systematic error and restricted to values greater than 0 to ensure stability of the fits. Details and results are given in the Supplement 1.

Besides temporal dimming, the series also provides spatial information of the plasmon propagation. As the first image of the series is mostly unaffected from bleaching, the plasmon propagation length follows from fitting the function

$$I(z) = D \exp(-Ez) \tag{2}$$

to the cross-section through the region unperturbed by the end spots (Fig. 2(a), black line). z is the lateral position. The result of $E = (0.32 \pm 0.03)\mu m^{-1}$ corresponds to a plasmon propagation length of $(3.1 \pm 0.3)\mu m$.

Further processing of these parameters leads to a spatial-dependent semi-logarithmic ratio $\ln(B/A)/E$. Figure 2(c) presents the result as a two-dimensional (2D) map for the selected pixels. The black line marks the region of substantial direct photon emission, which is unperturbed from the end spots. Figure 2(d) gives the one-dimensional $\ln(B/A)/E$ cross-section along this line. Over the whole length of the cross-section, the data points arrange along a constant function (solid line). Moderate oscillations of the data points take place, because of resonator effects due to the finite length of the nanowire [33], and Moiré effects due to the finite resolution of the

OPTICS CONTINUUM

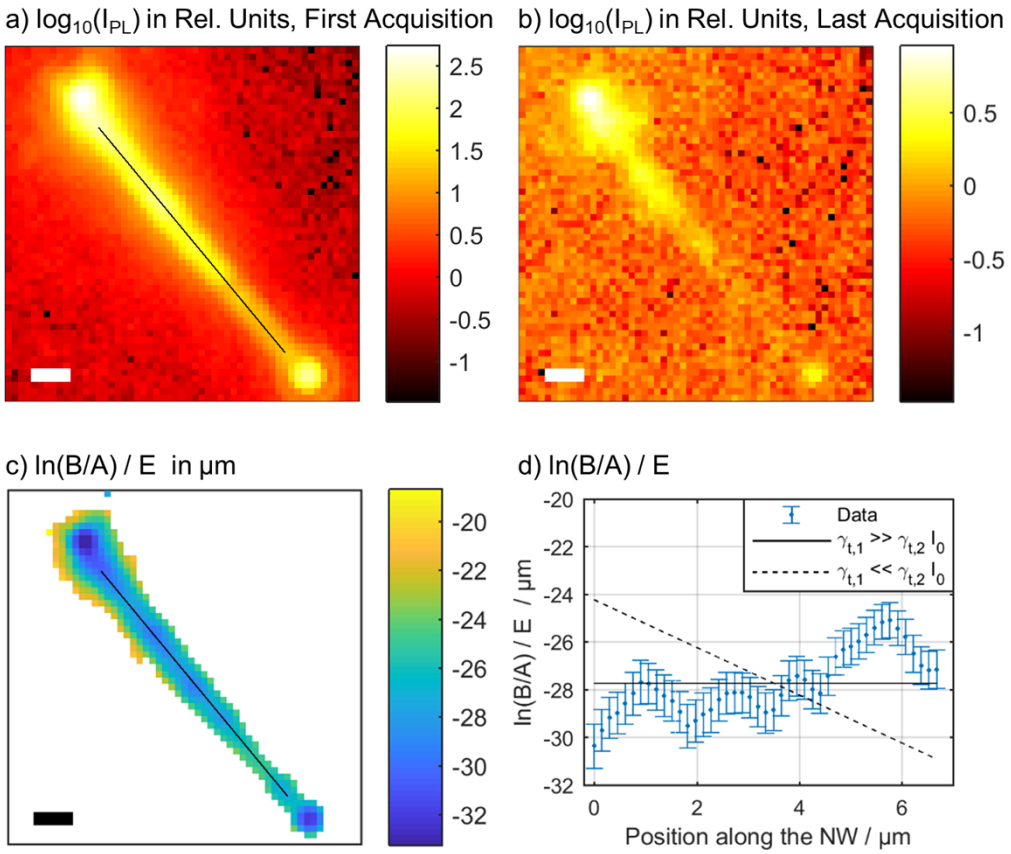

Fig. 2. Mapping of bleaching in a plasmon frequency converter. (a) PL image of the directly emitted photons from the MPDI molecules in the hybrid NW visualizes the plasmon intensity. (b) Upon bleaching the detected PL decreases. (c) All pixels, where substantial intensity is emitted, are used to analyze the bleaching through temporal fitting and comparison of the fit parameters, which are presented as 2D map of the semi-logarithmic ratio $\ln(B/A)/E$. (d) The plot of $\ln(B/A)/E$ along the cross-section through the 2D map in (c) (black line) reveals, that the bleaching cascade is triggered by a one-photon absorption. All scale bars measure 1 µm.

camera. The additional small steps of the datapoints at around 3.8 µm and 4.5 µm coincide with slight discontinuities in the PL image and are attributed to typical structural inhomogeneity of the core-shell system, e.g., grain boundaries in the Ag crystal structure, inhomogeneity of the dye molecule distribution or inhomogeneity of the amorphous silica shell itself.

According to our analytical model (see section 3, analytical model), a constant function occurs when the dominant bleaching cascade is triggered by a one-photon absorption process and scales linear with the excitation power. The scattered line shows a function with slope −1, which is expected when the bleaching cascade is triggered by a two-photon absorption process. As the data clearly deviates from this curve, a dominant two-photon absorption can be excluded as a trigger for the bleaching cascade. Consequently, the photobleaching rate from this particular building block was measured to be constant and cannot be further optimized by excitation power variations.

A more realistic scenario for a future device is the operation under ambient conditions. Especially the oxygen in the air is a candidate to influence the bleaching process [22,26–29]. The

OPTICS CONTINUUM

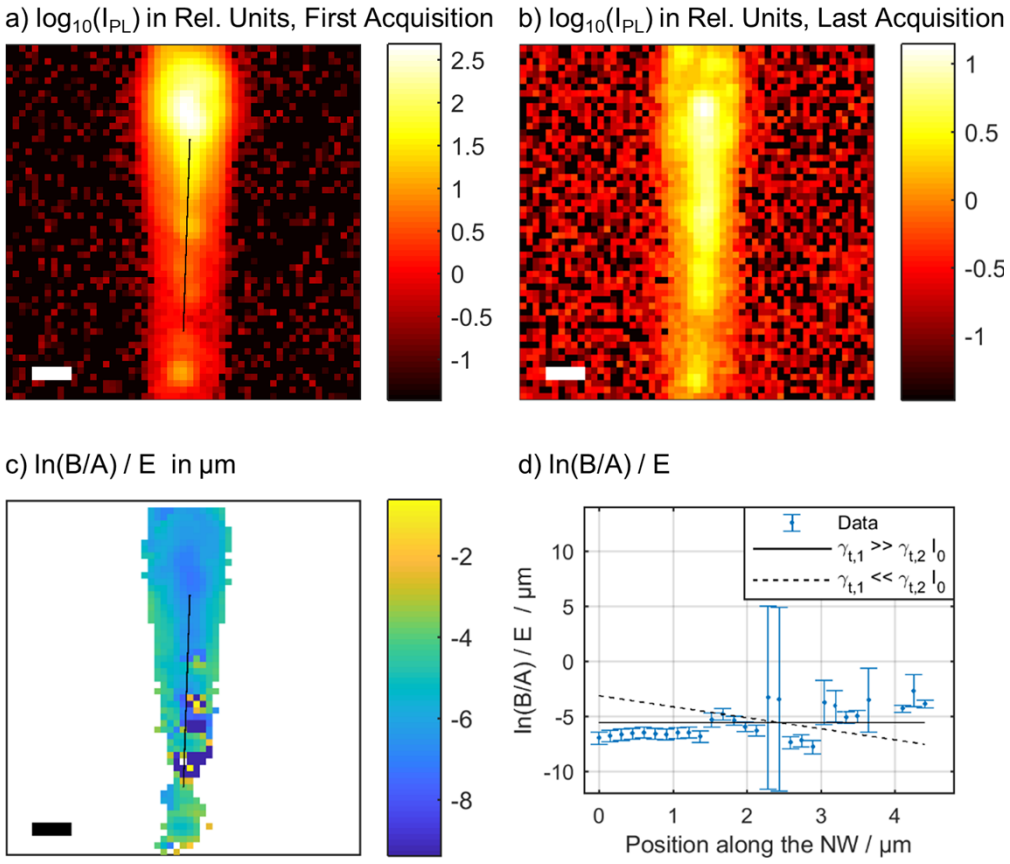

Fig. 3. Mapping of bleaching in a plasmon frequency converter under ambient conditions. (a) The PL of the first image follows the decaying excitation plasmon, but also shows inhomogeneity. (b) As before, upon bleaching the detected PL decreases. (c) The resulting 2D map of the semi-logarithmic ratio of the fit parameters $\ln(B/A)/E$ follows the trend of a constant function, but is affected by outliers. (d) The plot of $\ln(B/A)/E$ along the cross-section through the 2D map in (c) (black line) still reveals that the bleaching cascade is also triggered by a one-photon absorption. All scale bars measure 1 µm.

OPTICS CONTINUUM

PL of another NW was recorded using the same excitation power and acquisition settings as before. Figure 3(a) and (b) show the first and the last image of the series, respectively. The excitation laser was pointed on the upper end leading to PL, which follows the damped excitation plasmon along the NW (black line). As before, the opposite ends also appear as bright spots. Stronger as before, imperfections along the nanowire are visible in the first PL image. These imperfections arise probably from inhomogeneity on the surface of the nanowire, for example contaminations from the environment. For this nanowire, the pre-selection of the pixels is more crucial, in order to maintain stability of the temporal fits, and the results are less homogenous (see Supplement 1). The measured propagation length of the plasmon is $(0.68 \pm 0.04)\mu m$, corresponding to $E = (1.48 \pm 0.08)\mu m^{-1}$. The discrepancy to our first system lies within the expected deviation for this type of nanowires [33]. Figure 3(c) maps the fit-parameters in form of the semi-logarithmic ratio $\ln(B/A)/E$ and Fig. 3(d) gives the cross-section through the unperturbed region. It reveals a constant or slightly increasing distribution along the nanowire.

In consequence, even for this imperfect example under ambient conditions, the bleaching process was characterized to be triggered by a one-photon absorption. As before, the photobleaching rate is constant and cannot be optimized while operating this building block.

3. Analytical model

We define the end of our nanowires, where we excite the propagating plasmons with initial intensity I_0 (see Fig. 1(b)) as $z = 0$. While propagating along the NW (denoted as $+z$-direction) the plasmon is damped via Ohmic losses, described by a damping constant γ_z. Consequently, the plasmon intensity can be written as

$$I_{exc}(z) = I_0 \exp(-\gamma_z\, z) \tag{3}$$

Within the hybrid NW system, I_{exc} is the intensity of the plasmon which will be absorbed at a certain position by a molecule and will trigger a PL process. Based on a one-photon absorption process, the PL is proportional to I_{exc}. Furthermore, the detectable PL is proportional to an efficiency q, describing the probability that a photon is emitted and enters the optical detection path, and the amount ρ of active molecules within the detection area. Due to the on-going spatially-dependent bleaching of the molecules, ρ is position- and time-dependent. Thus, the detected intensity of the PL process is

$$I_{PL}(z,t) = \rho(z,t)\; q\; I_{exc}(z) \tag{4}$$

At the beginning, before any bleaching happened, the active molecules are spatially homogenously distributed, while the amount is vanishing for infinite long excitation:

$$\rho(z, t = 0) = \rho_0 \quad \text{and} \quad \rho\left(z, t \to \infty\right) = 0 \tag{5}$$

Figure 1(c) shows a calculated PL image at $t = 0$ where $I_{PL} \propto I_{exc}$.

In consequence, the whole time-dependence of the PL lies in the bleaching process. The time dependence of ρ at a certain position z is implicitly given by the proportionality between ρ and $\mathrm{d}\rho/\mathrm{d}t$. If the bleaching pathway in the Jablonski diagram is similar to the PL path (Fig. 1(a)), this process might be also linear and proportional to the excitation intensity I_{exc} with a time-constant $\gamma_{t,1}$.

$$\frac{\mathrm{d}\rho(z,t)}{\mathrm{d}t} = -\gamma_{t,1}\; I_{exc}(z)\; \rho(z,t) \tag{6}$$

In a hybrid system however, this is not necessarily the dominant process. If an additional bleaching process exists, $\mathrm{d}\rho/\mathrm{d}t$ must be expanded by an additional term. Here, we describe

OPTICS CONTINUUM

the possible case of a bleaching process triggered by simultaneous or consecutive two-photon absorption, a non-linear bleaching process. This is described by a second time-constant $\gamma_{t,2}$ and squared power-dependence, leading to

$$\frac{\mathrm{d}\rho(z,t)}{\mathrm{d}t} = -\gamma_{t,1}\, I_{exc}(z)\, \rho(z,t) - \gamma_{t,2}\, [I_{exc}(z)]^2\, \rho(z,t) \tag{7}$$

Together with the boundary conditions (Eq. (5)), this equation is solved by

$$\rho(z,t) = \rho_0 \cdot \exp(\, -\{\, \gamma_{t,1}\, I_{exc}(z) + \gamma_{t,2}\, [I_{exc}(z)]^2 \,\}\, t\,) \tag{8}$$

This gives the full spatio-temporal evolution of the detected PL intensity under the two competing bleaching processes.

$$I_{PL}(z,t) = q\ \rho_0\ I_0 \exp(-\gamma_z z) \exp[-\gamma_{t,1} I_0 \exp(-\gamma_z z) t]\ \exp[-\gamma_{t,2} I_0^2 \exp(-2\gamma_z z) t] \tag{9}$$

The consequence is, that the remaining active molecules at $t>0$ are differently distributed over the 1D system, depending on the bleaching time-constants (Fig. 4(a)). Figure 4(b) shows how the PL intensity changes from exponentially decaying at $t = 0$ (black) to a curve with its maximum almost at the end of the 1D system under linear bleaching (blue). For increasing (magenta) and dominating (red) non-linear bleaching, the contrast between the two ends of the system gets enhanced.

So, this effect can be used to gain insight into a general bleaching process from a PL measurement. Formula 9 shortens by applying certain conditions. Firstly, at a specific position z_i of the 1D-system, the PL intensity

$$I_{PL}(z_i,t) = q\ \rho_0\ I_0 \exp(-\gamma_z z_i) \exp\{-I_0 \exp(-\gamma_z z_i)\ [\gamma_{t,1} + \gamma_{t,2} I_0 \exp(-\gamma_z z_i)] t\} \tag{10}$$

reads as a simple exponential decay in time and can be written with constants A and B as

$$I_{PL}(z_i,t) = A \exp(-Bt) \tag{11}$$

Secondly, at the very beginning, at $t = 0$, the spatial distribution of the PL intensity directly follows the excitation intensity and becomes

$$I_{PL}(z, t=0) = q\ \rho_0\ I_0 \exp(-\gamma_z z) \tag{12}$$

which gives an exponential decay in space, using constants D and E,

$$I_{PL}(z, t=0) = D \exp(-Ez) \tag{13}$$

Combining these constants gives a spatial function, which type is strongly dependent on the underlying bleaching process

$$\frac{B}{A} = \frac{1}{q\rho_0}[\gamma_{t,1} + \gamma_{t,2} I_0 \exp(-Ez)] \tag{14}$$

The function B/A versus z appears as an exponential function with a decay constant according to the plasmon damping, a pre-factor defined by the non-linear bleaching rate, and an offset defined by the linear bleaching rate.

OPTICS CONTINUUM

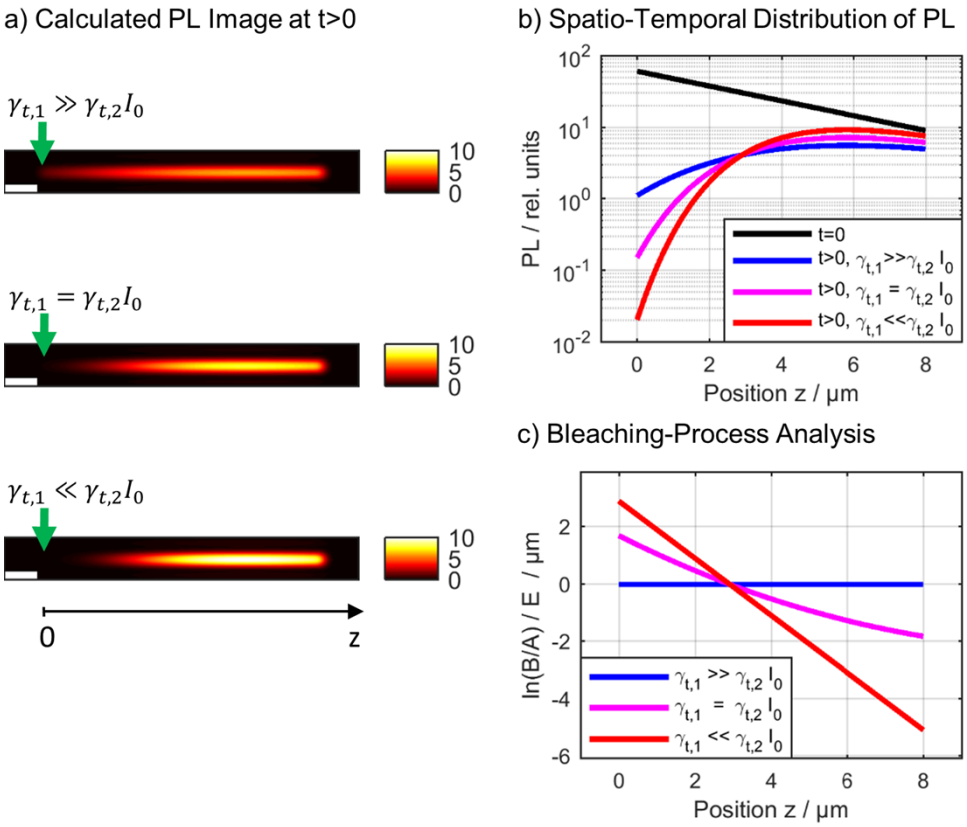

Fig. 4. Distribution of the PL under linear (dominated by bleaching rate $\gamma_{t,1}$) and non-linear (dominated by bleaching rate $\gamma_{t,2}$) bleaching. (a) After time t, parts of the molecules in the NW are bleached. The pattern in the PL image differs if only linear (up), both linear and non-linear (middle), or only non-linear bleaching (down) is considered. (b) The exponential pattern of the PL at t = 0 (black) changes due to bleaching for t > 0. A strong contrast occurs, if, additional to the linear bleaching (blue), also non-linear bleaching contributes (pink), or even dominates (red). (c) Comparing parameters A, B and E, results in a slope of 0 for linear bleaching (blue) or an integer slope (red), if non-linear bleaching dominates. Competing bleaching processes of equal strength results in a non-linear function (pink). All scale bars measure 1 µm.

OPTICS CONTINUUM

There are two limiting cases, where one of the two processes dominates. For linear bleaching ($\gamma_{t,1} \gg \gamma_{t,2} I_0$), the semi-logarithmic ratio $\ln(B/A)/E$ is a constant, or rather a linear function with slope 0:

$$\frac{\ln(B/A)}{E} \overset{\gamma_{t,1} \gg \gamma_{t,2} I_0}{\rightarrow} 0 \times z + \frac{1}{E} \ln\left(\frac{\gamma_{t,1}}{q\rho_0}\right) \tag{15}$$

For non-linear bleaching ($\gamma_{t,1} \ll \gamma_{t,2} I_0$), the semi-logarithmic ratio $ln(B/A)/E$ is a linear function with slope -1:

$$\frac{\ln(B/A)}{E} \overset{\gamma_{t,1} \ll \gamma_{t,2} I_0}{\rightarrow} (-1) \times z + \frac{1}{E} \ln\left(\frac{\gamma_{t,2} I_0}{q\rho_0}\right) \tag{16}$$

This slope is unitless and independent of any experimental-technical parameter or mathematical constant.

Consequently, the semi-logarithmic ratio $\ln(B/A)/E$ allows to define the dominant bleaching process, regardless of the optical system, or technical or environmental aspects (Fig. 4(c)).

4. Conclusion

In conclusion, we have introduced a plasmonic frequency converter as a prototypical nanophotonic element and presented a versatile and easy method for the assessment of its degradation. Based on a time series of PL images, we have found that the bleaching cascade in our hybrid MPDI / silver nanowire is dominated by processes following one-photon absorption. This means that the photobleaching rate is constant regardless of the plasmon converter operation. Our analytical model suggests a universal quantity, the semi-logarithmic ratio of easily accessible fit parameters, to discriminate possible bleaching cascades of photoemitters within a one-dimensional hybrid device. This opens the door for easy degradation monitoring and paves the way for in-operando optimization of hybrid nanophotonic circuits.

Funding. Deutsche Forschungsgemeinschaft (182087777-SFB 951).

Acknowledgments. Funding by the Deutsche Forschungsgemeinschaft (DFG), Project No. 182087777-SFB 951 (project B2) is acknowledged.

Disclosures. The authors declare no conflicts of interest.

Data availability. Data underlying the results presented in this paper are not publicly available at this time but may be obtained from the authors upon reasonable request.

Supplemental document. See Supplement 1 for supporting content.

References

1. A. W. Elshaari, W. Pernice, K. Srinivasan, O. Benson, and V. Zwiller, "Hybrid integrated quantum photonic circuits," Nat. Photonics **14**(5), 285–298 (2020).
2. M. Decker and I. Staude, "Resonant dielectric nanostructures: A low-loss platform for functional nanophotonics," J. Opt. **18**(10), 103001 (2016).
3. C. Zou, J. Sautter, F. Setzpfandt, and I. Staude, "Resonant dielectric metasurfaces: Active tuning and nonlinear effects," J. Phys. D: Appl. Phys. **52**(37), 373002 (2019).
4. H. Sugimoto and M. Fujii, "Colloidal mie resonant silicon nanoparticles," Nanotechnology **32**(45), 452001 (2021).
5. H. Yu, Y. Peng, Y. Yang, and Z.-Y. Li, "Plasmon-enhanced light–matter interactions and applications," npj Comput. Mater. **5**(1), 45 (2019).
6. N. Jiang, X. Zhuo, and J. Wang, "Active plasmonics: Principles, structures, and applications," Chem. Rev. **118**(6), 3054–3099 (2018).
7. F. Marquier, C. Sauvan, and J.-J. Greffet, "Revisiting quantum optics with surface plasmons and plasmonic resonators," ACS Photonics **4**(9), 2091–2101 (2017).
8. D. K. Gramotnev and S. I. Bozhevolnyi, "Plasmonics beyond the diffraction limit," Nat. Photonics **4**(2), 83–91 (2010).
9. W. L. Barnes, A. Dereux, and T. W. Ebbesen, "Surface plasmon subwavelength optics," Nature (London, U. K.) **424**(6950), 824–830 (2003).
10. J. Takahara, S. Yamagishi, H. Taki, A. Morimoto, and T. Kobayashi, "Guiding of a one-dimensional optical beam with nanometer diameter," Opt. Lett. **22**(7), 475–477 (1997).

OPTICS CONTINUUM

11. R. M. Dickson and L. A. Lyon, "Unidirectional plasmon propagation in metallic nanowires," J. Phys. Chem. B **104**(26), 6095–6098 (2000).
12. M. Allione, V. V. Temnov, Y. Fedutik, U. Woggon, and M. V. Artemyev, "Surface plasmon mediated interference phenomena in low-q silver nanowire cavities," Nano Lett. **8**(1), 31–35 (2008).
13. H. Ditlbacher, A. Hohenau, D. Wagner, U. Kreibig, M. Rogers, F. Hofer, F. R. Aussenegg, and J. R. Krenn, "Silver nanowires as surface plasmon resonators," Phys. Rev. Lett. **95**(25), 257403 (2005).
14. G. Mie, "Beiträge zur optik trüber medien, speziell kolloidaler metallösungen," Ann. Phys. (Berlin, Ger.) **330**(3), 377–445 (1908).
15. H. Siampour, S. Kumar, and S. I. Bozhevolnyi, "Nanofabrication of plasmonic circuits containing single photon sources," ACS Photonics **4**(8), 1879–1884 (2017).
16. C. Schörner, S. Adhikari, and M. Lippitz, "A single-crystalline silver plasmonic circuit for visible quantum emitters," Nano Lett. **19**(5), 3238–3243 (2019).
17. M. Rothe, Y. Zhao, J. Müller, G. Kewes, C. T. Koch, Y. Lu, and O. Benson, "Self-assembly of plasmonic nanoantenna–waveguide structures for subdiffractional chiral sensing," ACS Nano **15**(1), 351–361 (2021).
18. C. Toninelli, I. Gerhardt, A. S. Clark, A. Reserbat-Plantey, S. Götzinger, Z. Ristanović, M. Colautti, P. Lombardi, K. D. Major, I. Deperasińska, W. H. Pernice, F. H. L. Koppens, B. Kozankiewicz, A. Gourdon, V. Sandoghdar, and M. Orrit, "Single organic molecules for photonic quantum technologies," Nat. Mater. **20**(12), 1615–1628 (2021).
19. S. Kumar, S. K. H. Andersen, and S. I. Bozhevolnyi, "Extremely confined gap-plasmon waveguide modes excited by nitrogen-vacancy centers in diamonds," ACS Photonics **6**(1), 23–29 (2019).
20. G. Kewes, M. Schoengen, O. Neitzke, P. Lombardi, R.-S. Schönfeld, G. Mazzamuto, A. W. Schell, J. Probst, J. Wolters, B. Löchel, C. Toninelli, and O. Benson, "A realistic fabrication and design concept for quantum gates based on single emitters integrated in plasmonic-dielectric waveguide structures," Sci. Rep. **6**(1), 28877 (2016).
21. J. Vogelsang, R. Kasper, C. Steinhauer, B. Person, M. Heilemann, M. Sauer, and P. Tinnefeld, "A reducing and oxidizing system minimizes photobleaching and blinking of fluorescent dyes," Angew. Chem. Int. Ed. **47**(29), 5465–5469 (2008).
22. M. Haase, C. G. Hubner, F. Nolde, K. Mullen, and T. Basche, "Photoblinking and photobleaching of rylene diimide dyes," Phys. Chem. Chem. Phys. **13**(5), 1776–1785 (2011).
23. H. Cang, Y. Liu, Y. Wang, X. Yin, and X. Zhang, "Giant suppression of photobleaching for single molecule detection via the purcell effect," Nano Lett. **13**(12), 5949–5953 (2013).
24. K. Vasilev, F. D. Stefani, V. Jacobsen, W. Knoll, and M. Kreiter, "Reduced photobleaching of chromophores close to a metal surface," The Journal of Chemical Physics **120**(14), 6701–6704 (2004).
25. D. Solis, W.-S. Chang, B. P. Khanal, K. Bao, P. Nordlander, E. R. Zubarev, and S. Link, "Bleach-imaged plasmon propagation (blipp) in single gold nanowires," Nano Lett. **10**(9), 3482–3485 (2010).
26. J. Lub, P. A. van Hal, R. Smits, L. Malassenet, J. Pikkemaat, and R. A. M. Hikmet, "On the photo-oxidation of perylene bisimide dyes in alcoholic solutions," J. Lumin. **207**, 585–588 (2019).
27. J. Lub, P. A. van Hal, E. M. G. Custers, H. H. Knobel, and R. A. M. Hikmet, "Photo-substitution reactions of perylene red dyes," J. Lumin. **218**, 116845 (2020).
28. M. Xie, D. Hong, S. Wan, M. Xie, and Y. Tian, "Enhancement of photostability and fluorescence quantum yield of dxp in solid state by using mixed solvent," Chem. Phys. Lett. **717**, 119–123 (2019).
29. H. Piwoński, A. Sokołowski, and J. Waluk, "In search for the best environment for single molecule studies: Photostability of single terrylenediimide molecules in various polymer matrices," J. Phys. Chem. Lett. **6**(13), 2477–2482 (2015).
30. E. M. Purcell, "Proceedings of the american physical society," Phys. Rev. **69**(1-2), 37–38 (1946).
31. O. S. Ojambati, W. M. Deacon, R. Chikkaraddy, C. Readman, Q. Lin, Z. Koczor-Benda, E. Rosta, O. A. Scherman, and J. J. Baumberg, "Breaking the selection rules of spin-forbidden molecular absorption in plasmonic nanocavities," ACS Photonics **7**(9), 2337–2342 (2020).
32. P. Jiang, T. Schroeder, M. Bath, V. Lesnyak, N. Gaponik, A. Eychmüller, and O. Benson, "Incoherent photon conversion in selectively infiltrated hollow-core photonic crystal fibers for single photon generation in the near infrared," Opt. Express **20**(10), 11536–11547 (2012).
33. M. Rothe, Y. Zhao, G. Kewes, Z. Kochovski, W. Sigle, P. A. van Aken, C. Koch, M. Ballauff, Y. Lu, and O. Benson, "Silver nanowires with optimized silica coating as versatile plasmonic resonators," Sci. Rep. **9**(1), 3859 (2019).